Cost effective green synthesis of NiO nanostructures as highly efficient photocatalysts for degradation of organic dyes

Hameed Ullah ✉, *Lubna Mushtaq, Zia Ullah, Masroor Ahmad Bangesh, Mohsan Nawaz*

Department of Chemistry, Hazara University, Mansehra, 21300, Pakistan
✉ *E-mail: hameedwazir@yahoo.co.uk*

Published in Micro & Nano Letters; Received on 28th April 2018; Revised on 12th September 2018; Accepted on 1st October 2018

Here, the cost effective green synthesis of nickel oxide (NiO) nanostructures has been reported. The organic capping and/or reducing agents were obtained by extraction from wastes of three different vegetables (cauliflower, potatoes and peas). The extracts of cauliflower and peas peels gave nanowhiskers while the extract of potato peels gave nanorods of NiO, as confirmed by scanning electron microscopy. X-ray diffraction analyses demonstrated the nanocrystalline cubic phase of NiO in all the samples. However, crystallite size varied with the extract of vegetable waste used. Fourier transform infrared analysis helps in identifying different vibrations, particularly Ni–O stretching vibrations, and diffuse reflectance spectra analyses led to the establishment of bandgap energies. The resulting NiO nanostructures were tested for their efficiencies as photocatalysts for Methylene blue degradation. All the three samples have shown significant photocatalytic activities. The exploration in this study clearly demonstrates the very high photocatalytic activities of the synthesised NiO nanostructures, which can be used as competent agents for treatment of wastewater to remove toxic dyes.

1. Introduction: Nickel oxide (NiO) is among the p-type semiconducting oxides with a wide bandgap of 3.6–4.0 eV, depending upon the nature of defects and their density [1]. It is among the antiferromagnetic materials having Neel's temperature (T_N) of ∼523 K, and despite of having a high isoelectric point of ∼10.7, it shows high ionisation. Nowadays, NiO nanoparticles (NPs) are studied widely owing to their excellent electrocatalysis properties, high-chemical stability, super conductivity, and electron transfer capability at the nanometre level scale [2]. NiO NPs have been found potential applications in different areas, for example, in water treatment, catalysis, gas and chemical sensors, magnetic and electrochromic devices, battery and photovoltaic devices, and antimicrobial activities [1]. Numerous synthesis methods have been adopted to fabricate NiO NPs in a range of sizes. These various methods include but not limited to solvothermal [3], precipitation–calcination [4], chemical precipitation [5], microwave-assisted hydrothermal [6], and thermal decomposition [7]. However, these methods involve complicated procedures, harmful chemicals, and complex apparatuses. Therefore, following the basic principles of green chemistry, alternate synthesis methods which are simple, cost effective, and above all environment friendly have been employed for synthesis of metal oxide NPs [8, 9]. The environmentally benign synthesis approach i.e. a green synthesis method has also been used for preparation of NiO NPs [10].

These recent researches are mostly focused on the synthesis of NPs using plant extracts, and thus opened an era of nontoxic methods for the production of NPs. The plants for the synthesis of NPs readily supply extracts, which are best-known natural capping and/or reducing agents. It has been reported that plant extracts have a potential influence on the morphology and particle size distribution of the resulting NPs. The morphology and the particle size distribution in turn affect the magnitude of the bandgap [11]. Also it is well known that the bandgap has a strong influence on the conductivity and chemical reactivity of NPs [12]. The biogenic methods for NP synthesis will be made further cost effective, if vegetable wastes are used as sources of extracts. Since, hundred thousand tonnes of vegetable wastes are produced each day, and thus available locally at low cost or even cost free. The extracts from these vegetable wastes for the synthesis of NPs can dramatically lower the production costs of the resulting nanomaterials.

Here we report upon biogenic synthesis of NiO NPs using vegetable (cauliflowers, potatoes and peas) waste extracts, which with surface directing properties have an appreciable hold on the morphology of the resulting NiO NPs. The recent research activities highlight the importance of heterogeneous photocatalysis, having the potential to efficiently degrade the organic contaminants in the atmospheric and aquatic environments [13]. The process involves sunlight and semiconducting photocatalysts to accelerate the degradation or destruction of the toxic organic pollutants [14, 15]. However, efficiencies of photocatalysts stringently depend upon their nature, composition and particularly the morphology, which have been effectively controlled by employing structure directing and/or capping agents (SDAs). We have controlled the morphology by using extracts of cost effective vegetable wastes i.e. cauliflower waste, and potato and peas peels. The resulting NiO nanostructures have shown remarkable efficiencies as photocatalysts for degradation of Methylene blue (MB) dye which was taken as test case.

2. Experimental

2.1. Materials: We have used analytical grade chemicals without further purifications and/or treatments. The nickel source, nickel nitrate hexahydrate ($Ni(NO_3)_2{\cdot}6H_2O$)), was purchased from Riedel-de Häen and MB was purchased from a commercial supplier of the company Sigma-Aldrich. We have collected the wastes of vegetables i.e. cauliflower (*Brassica oleracea*), and potato (*Solanum tuberosum*) and peas (*Pisum sativum*) peels from a local market. Deionised water was prepared in our own laboratory.

2.2. Synthesis of NiO nanostructures: The extracts of the vegetable wastes were prepared by a simple method following a reported procedure [16]. In a typical preparation protocol, we have taken 50 g of the vegetable waste, which was washed thoroughly with deionised water. The well-washed vegetable waste was dried and then was grinded. The ground vegetable waste was dispersed in 1000 mL of deionised water, and was mechanically stirred for a given time. The solid was filtered off and the filtrate was collected in a clean flask. To synthesise the NiO NPs, each individual extract of cauliflower waste, and potato and peas peels was added to an aqueous solution of $Ni(NO_3)_2{\cdot}6H_2O$. Afterwards, the pH of each solution was adjusted to 10 by adding NaOH solution. The resulting reaction

mixture was stirred for 24 h at 60°C, and the precipitates were thoroughly washed with deionised water several times. The powder was dried at 80°C in a laboratory oven, and the solid powders collected from the cauliflower waste, potato peels and peas peels were labelled as N-1, N-2, and N-3, respectively. The NiO samples N-1, N-2, and N-3 were calcined at 500°C for 3 h to remove any organic impurities left after washing.

2.3. Photocatalytic degradation of MB dye: The synthesised NiO NPs i.e. N-1, N-2, and N-3 were used as photocatalysts for photo-induced degradation of MB dye. A typical photocatalysis experiment involves a solution (1.0×10^{-5} M) of MB dye prepared by dissolving 0.02 g of dye in the required amount of deionised water. One hundred millilitre of the MB dye solution was taken from this stock solution and 0.25 g of NiO NPs was added. The photocatalyst containing dye solution was sonicated for 5 min, kept under constant stirring for 30 min in the dark to establish the equilibrium between adsorption and desorption. An aliquot was taken off this solution, and analysed using a UV-Vis spectrophotometer to obtain its absorption spectrum. This sample was termed blank. Afterwards, a high-pressure Hg lamp (emission at 365 nm) was erected parallel to the solution flask, and the lamp was switched on to irradiate the solution. Aliquots were taken at every 30 min interval for analyses using the UV-Vis spectrophotometer while the solution was under constant stirring and irradiation.

2.4. Characterisation: The crystal structure, composition, and crystallite size were determined by using a PANalytical (X'pert-PRO) diffractometer, which was equipped with Cu K_α having average X-ray wavelength of 1.542 Å. The diffracted X-ray beams were detected using an X'celerator detector, which was circling at a step size of 0.0840 2θ and counting time of 180 s. The Fourier transform infrared (FTIR) spectra were recorded in ATR mode using SMARTORBIT of the Thermo Electron Corporation FTIR spectrophotometer. We have employed a scanning electron microscope (SEM; JSM-5910) to study the morphology of the resulting samples. A Lambda 950 UV-Vis spectrophotometer from PerkinElmer Inc. was used to record the diffuse reflectance spectra (DRS) of all the three samples. The MB dye degradation under UV-Vis radiation was followed by measuring its spectra using a PerkinElmer Inc. (Model; Lambda 950) spectrophotometer.

3. Results and discussion: The NiO samples N-1, N-2, and N-3 were analysed by different analytical tools to establish their microstructures and morphologies. The powder X-ray diffraction (XRD) patterns of N-1, N-2, and N-3 samples are presented in Fig. 1. The XRD patterns of all the samples N-1, N-2, and N-3 show two distinct peaks at 2θ around 37.38° and 43.48° which correspond to the

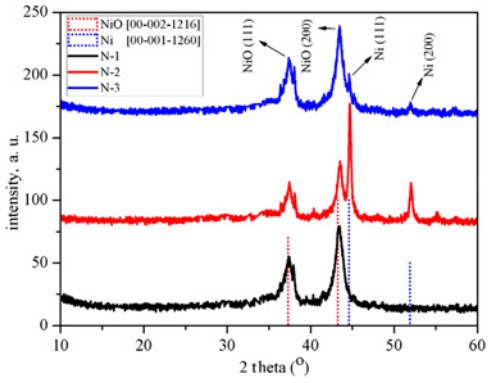

Fig. 1 *XRD diffractograms of NiO NPs synthesised by using vegetable waste extracts of cauliflower (N-1), and potato (N-2) and peas (N-3) peels*

reflection planes (111) and (200), respectively. The search and match performed using X'pert Highscore software shows that these crystallographic planes i.e. (111) and (200) in the XRD patterns of N-1, N-2, and N-3 samples match with those of the standard NiO in its cubic crystal system given in the Joint Committee for Powder Diffraction Standards (JCPDS) database through powder diffraction file (PDF) number 00-002-1216. The peaks are comparatively broader indicating the formation of crystallites in the nanometre level scale. The crystallite sizes were measured by Scherrer's formula which is given in (1):

$$D = K\lambda/\beta\cos\theta \tag{1}$$

where D, K, λ, β, and θ stand for the average crystallite size, Scherrer constant (0.89), wavelength of the X-rays (Cu $K_\alpha = 1.542$ Å), angle of diffraction, and the full width of the peak at half maximum (FWHM), respectively. The average crystallite sizes are 15.25, 21.50, and 24.15 nm, respectively, for N-1, N-2, and N-3 samples (Table 1). It is evident from the data given in Table 1 that the crystallite size varies significantly by varying the capping agent (extract). The smallest crystallite size was obtained by using cauliflower waste extract (N-1) followed by potato peel extract (N-2) and the largest crystallite size was observed for peas peel extract (N-3).

Beside the peaks for NiO, the XRD patterns of N-2 and N-3 show additional peaks at 2θ of 44.64° and 52.03° which correspond, respectively, to the reflections from crystallographic planes (111) and (200) of Ni in its cubic crystal system. This was confirmed by matching with the standard Ni pattern given in the JCPDS database through PDF no. 00-001-1260. The average crystallite sizes of Ni were measured to be 38.65 and 54.35 nm for N-2 and N-3 samples, respectively, employing Scherrer's formula (1). The peaks for Ni are not observed in the XRD pattern of N-1, and the Ni peaks are lower intense in the XRD pattern of N-3. The existence of Ni could be explained on the assumption that the vegetable extracts may possess some reducing agents, which reduce the Ni^{2+} to Ni [17]. Subsequently, the as-synthesised Ni was oxidised in the calcination process to NiO. The nearly complete conversion of Ni to NiO in the case of N-1 and N-3, and partial conversion in the case of N-2 could be corresponded to the very smaller diameters of nanowhiskers and large diameters of nanorods, respectively. In fact, the larger the diameter of nanostructures, the more they have resistance to thermal oxidation and vice versa.

FTIR spectra of N-1, N-2, and N-3 samples were obtained in the range of 4000–400 cm^{-1}, and the pertinent data are presented in Table 1. The FTIR spectra show a weak but broad peak in the range of 3200–3400 cm^{-1}. This peak corresponds to the O–H stretching vibration due to adsorbed water molecules. Peaks peculiar of Ni–O vibrations appear in the FTIR spectra of all the samples in the range of 750–400 cm^{-1} [18, 19]. The blue shift in the FTIR vibrations of Ni–O bond compared with that of bulk could be corresponded to the quantum confinement at the nanoscale [20].

SEM micrographs of N-1, N-2, and N-3 samples are presented in Fig. 2. As shown in Fig. 2*a*, N-1 contains uniformly distributed whisker-like nanostructures. The nanowhiskers are self-assembled into chiral nematic liquid crystalline-like structures (Fig. 2*b*). The nanowhiskers in N-1 are nonuniform longitudinally. Contrary to N-1, the SEM micrograph (Fig. 2*c*) of N-2 shows rod-like structures, which are self-assembled through longitudinal edges. The larger rods seem to be formed of nanowhiskers which are aligned longitudinally to each other (Fig. 2*d*). The SEM micrograph, given in Fig. 2*e*, of N-3 shows nanowhiskers as were seen in the case of N-1. However, the nanowhiskers in this case seem to be round and pointing (Fig. 2*f*).

To know the bandgap energies of N-1, N-2, and N-3 sample, DRS spectra were recorded, and are presented in Fig. 3 which

doi: 10.1049/mnl.2018.5106

Table 1 Pertinent data from FTIR, XRD, and DRS results of NiO NPs

Sample	FTIR frequency, cm^{-1}			XRD	DRS
	ν(Ni–O)	ν(Ni–O)	ν(Ni–O)	Crystallite size, nm	Energy bandgap, eV
N-1	426	586	711	15.25	4.810
N-2	425	583	644	21.50	4.932
N-3	425	600	650	24.15	4.973

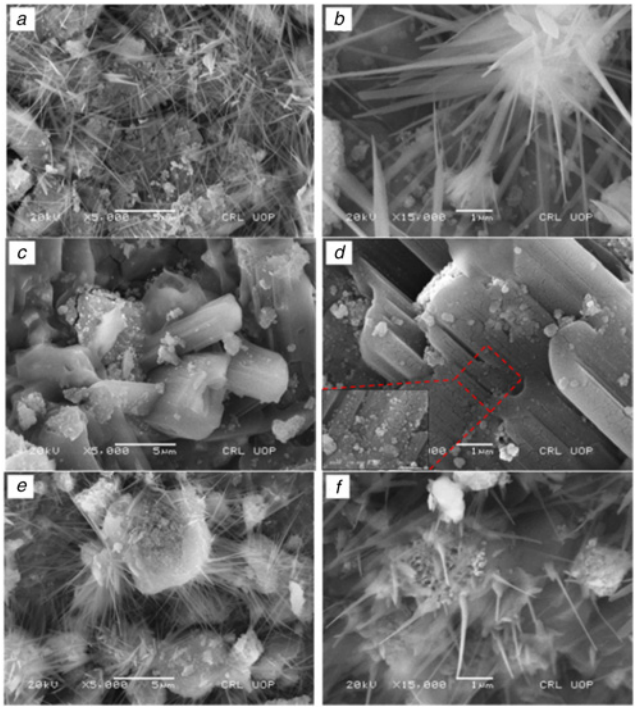

Fig. 2 *SEM micrographs of NiO NP samples synthesised by using extracts of cauliflower waste, potato peels and peas peels, respectively*
a, b N-1
c, d N-2
e, f N-3

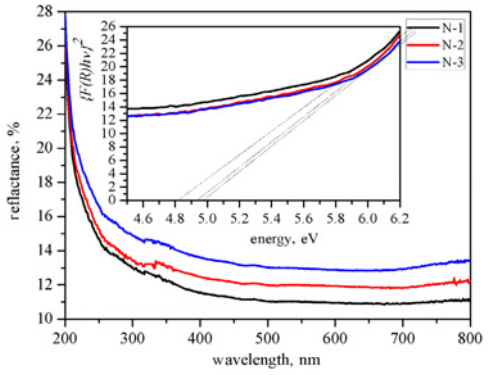

Fig. 3 *DRS spectra of N-1, N-2, and N-3, and Kubelka–Munk function plot vs. hν (inset)*

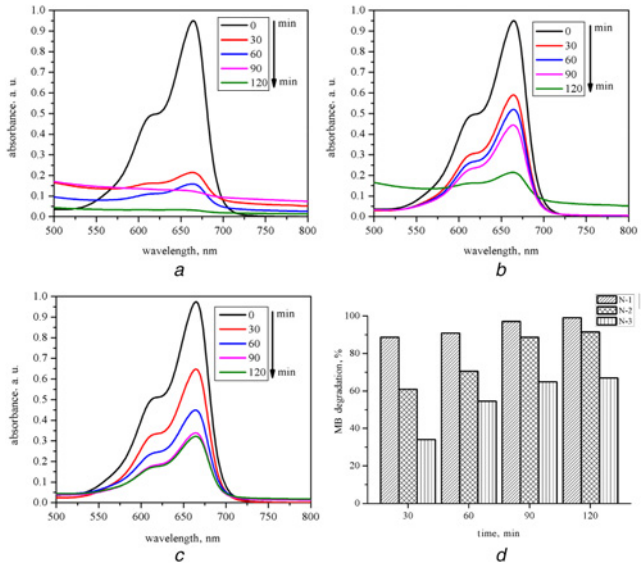

Fig. 4 *UV-Vis absorption spectra of the MB dye solution (1×10^{-5} M) in the presence of NiO photocatalysts, and bar graph showing decomposition of MB dye in percent as a function of irradiation time in the presence of NiO photocatalysts*
a N-1
b N-2
c N-3
d N-1, N-2, and N-3

show that the three samples absorb nearly similarly. The direct energy bandgaps were measured by plotting the Kubelka–Munk function ($\{F(R)h\upsilon\}^2$) against the photon energy ($h\upsilon$), and the plots are presented as an inset in Fig. 3. The energy bandgaps determined by extrapolating the straight portion of plots down to zero are 4.810, 4.932, and 4.973 eV for N-1, N-2, and N-3 samples, respectively. The bandgap energies are larger than those of bulk NiO [21]. The increased bandgaps can be justified by the nanosisation of the NiO particles.

The obtained NiO nanostructures, N-1, N-2, and N-3, were tested to find their photocatalytic efficiencies. As could be seen in Fig. 4, series of UV-Vis spectra, the maximum absorption peak around 665 nm of MB depletes after irradiation with the UV lamp, indicating photo-induced degradation of the test case dye. In fact, the dye degradation is owed to the redox reaction mechanism which involves holes and electrons undergoing successive oxidation and reduction, respectively, with organic species, here in this case MB dye [22]. The organic species aimed to be degraded might be adsorbed at the surface of the heterogeneous photocatalyst, NiO nanostructures here in our case, to initiate and finally complete the degradation reactions [22]. The degradation rate of MB dye is faster in the beginning, i.e. in the time span of zero to 30 min, and then becomes slow. The decrease in dye degradation rate could be corresponded to the dilution factor. It is also pertinent to mention here that the degradation rate in this first 30 min is far higher in the case of N-1 photocatalyst followed by N-2 and the least is observed for N-3. Likewise, the percent degradation of MB dye at the end of 120 min is the largest for the N-1 photocatalyst (~99%) followed by N-2 (~91.5%) and the least is observed for N-3 (~67%) as depicted by the bar graph presented in Fig. 4*d*.

To know the MB dye degradation as a function of time, the ratio of concentration after each interval of 30 min (C_t) to the initial

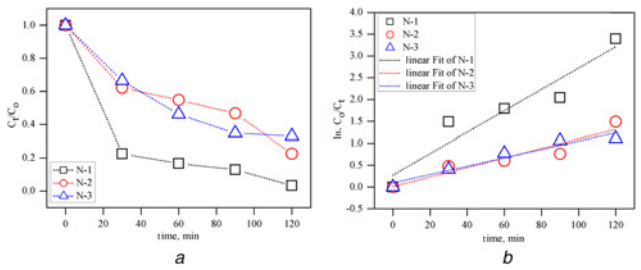

Fig. 5 *Plots as a function of time*
a C_t/C_0
b $ln(C_0/C_t)$

concentration (C_0) is plotted as a function of irradiation time (Fig. 5*a*). As shown by the graph, the MB dye degradation is faster and higher while using N-1 sample as the photocatalyst, and sluggish as well as lower when N-2 and N-3 samples are employed as photocatalysts. The MB dye degradation reaction rate was determined by following the previously derived formula (2) [23]:

$$\ln\left(\frac{C_0}{C_t}\right) = k \cdot t \tag{2}$$

In (2), the terms C_0, C_t, k, and t are used to represent the initial concentration, concentration at time 't', rate constant, and irradiation time, respectively. The plot of $\ln(C_0/C_t)$ *vs.* time is presented in Fig. 5*b* which shows a straight line, indicating that the MB dye degradation is a pseudo-first-order reaction [23].

4. Conclusion: In summary, we have synthesised NiO nanostructures in different morphologies by a simple green synthesis method, which is environment friendly and cost effective. The microstructure and morphology investigations revealed that the vegetable waste extracts contain efficient SDAs. Furthermore, the variation in morphology revealed that the different vegetable waste extracts contain SDAs of different natures. The cubic phase NiO nanostructures possessed longitudinally nonuniform whiskers like morphology when the cauliflower waste and peas peel extracts were use. On the other hand, self-assembled nanorods were achieved by using potato peel extract. The heterogeneous photocatalysts thus obtained have shown very high photo-induced MB dye degradation activities. The NiO nanostructures obtained by using cauliflower waste extract have degraded ~99% of MB dye in 120 min followed by those obtained with potato (~91.5) and peas (~67%) peel extracts.

5. Acknowledgments: The authors acknowledge the financial supports provided by the higher education commission (HEC) of Pakistan under the national research program for universities (NRPU) through grant no. 20-2784/NRPU/R&D/HEC/13, and access to scientific instrumentations program (ASIP).

6 References

[1] Harraz F., Mohamed R., Shawky A., *ET AL.*: 'Composition and phase control of Ni/NiO nanoparticles for photocatalytic degradation of EDTA', *J. Alloys Compd.*, 2010, **508**, (1), pp. 133–140

[2] Thema F., Manikandan E., Gurib-Fakim A., *ET AL.*: 'Single phase bunsenite NiO nanoparticles green synthesis by *Agathosma betulina* natural extract', *J. Alloys Compd.*, 2016, **657**, pp. 655–661

[3] Ghosh M., Biswas K., Sundaresan A., *ET AL.*: 'MnO and NiO nanoparticles: synthesis and magnetic properties', *J. Mater. Chem.*, 2006, **16**, (1), pp. 106–111

[4] Deng X., Chen Z.: 'Preparation of nano-NiO by ammonia precipitation and reaction in solution and competitive balance', *Mater. Lett.*, 2004, **58**, (3–4), pp. 276–280

[5] Mahaleh Y., Sadrnezhaad S., Hosseini D.: 'NiO nanoparticles synthesis by chemical precipitation and effect of applied surfactant on distribution of particle size', *J. Nanomater.*, 2008, **2008**, p. 78

[6] Zhu Z., Wei N., Liu H., *ET AL.*: 'Microwave-assisted hydrothermal synthesis of $Ni(OH)_2$ architectures and their in situ thermal convention to NiO', *Adv. Powder Technol.*, 2011, **22**, (3), pp. 422–426

[7] Zhang X., Shi W., Zhu J., *ET AL.*: 'Synthesis of porous NiO nanocrystals with controllable surface area and their application as supercapacitor electrodes', *Nano Res.*, 2010, **3**, (9), pp. 643–652

[8] Hoseinpour V.: 'Green synthesis, characterization, and photocatalytic activity of manganese dioxide nanoparticles', *Micro Nano Lett.*, 2018, **14**, p. 104

[9] Souri M., Hoseinpour V., Shakeri A., *ET AL.*: 'Optimisation of green synthesis of MnO nanoparticles via utilising response surface methodology', *IET Nanobiotechnol.*, 2018, **12**, (6), pp. 822–827

[10] Ezhilarasi A.A., Vijaya J.J., Kaviyarasu K., *ET AL.*: 'Green synthesis of NiO nanoparticles using *Moringa oleifera* extract and their biomedical applications: cytotoxicity effect of nanoparticles against HT-29 cancer cells', *J. Photochem. Photobiol. B, Biol.*, 2016, **164**, pp. 352–360

[11] Rodriguez J.A., Chaturvedi S., Kuhn M., *ET AL.*: 'Reaction of H_2S and S_2 with metal/oxide surfaces: band-gap size and chemical reactivity', *J. Phys. Chem. B*, 1998, **102**, (28), pp. 5511–5519

[12] Hoffman R.: 'Solids and surfaces: A chemist's view of bonding in extended structures' (Cornell Univ., Ithaca, NY, Baker Lab, 1988)

[13] Pizarro P., Guillard C., Perol N., *ET AL.*: 'Photocatalytic degradation of imazapyr in water: comparison of activities of different supported and unsupported TiO_2-based catalysts', *Catal. Today*, 2005, **101**, (3–4), pp. 211–218

[14] Yates H., Nolan M., Sheel D., *ET AL.*: 'The role of nitrogen doping on the development of visible light-induced photocatalytic activity in thin TiO_2 films grown on glass by chemical vapour deposition', *J. Photochem. Photobiol. A, Chem.*, 2006, **179**, (1–2), pp. 213–223

[15] Ni M., Leung M.K., Leung D.Y., *ET AL.*: 'A review and recent developments in photocatalytic water-splitting using TiO_2 for hydrogen production', *Renew. Sust. Energy Rev.*, 2007, **11**, (3), pp. 401–425

[16] Ullah H., Ullah Z., Fazal A., *ET AL.*: 'Use of vegetable waste extracts for controlling microstructure of CuO nanoparticles: green synthesis, characterization, and photocatalytic applications', *J. Chem.*, 2017, **2017**, pp. 1–5

[17] Duan H., Wang D., Li Y.: 'Green chemistry for nanoparticle synthesis', *Chem. Soc. Rev.*, 2015, **44**, (16), pp. 5778–5792

[18] Li J., Zhao F., Zhang L., *ET AL.*: 'Electrospun hollow ZnO/NiO heterostructures with enhanced photocatalytic activity', *RSC Adv.*, 2015, **5**, (83), pp. 67610–67616

[19] Rahimi R., Bozorgpour M., Rabbani M.: 'Photocatalytic degradation of MB from water by using Ni-TPPS/NiO nanoparticles'

[20] Kaviyarasu K., Manikandan E., Kennedy J., *ET AL.*: 'Synthesis and characterization studies of NiO nanorods for enhancing solar cell efficiency using photon upconversion materials', *Ceram. Int.*, 2016, **42**, (7), pp. 8385–8394

[21] Thota S., Shim J., Seehra M.: 'Size-dependent shifts of the Néel temperature and optical band-gap in NiO nanoparticles', *J. Appl. Phys.*, 2013, **114**, (21), p. 214307

[22] Ajmal A., Majeed I., Malik R.N., *ET AL.*: 'Principles and mechanisms of photocatalytic dye degradation on TiO_2 based photocatalysts: A comparative overview', *RSC Adv.*, 2014, **4**, (70), pp. 37003–37026

[23] Yetim T., Tekin T.: 'A kinetic study on photocatalytic and sonophotocatalytic degradation of textile dyes', *Period. Polytech., Chem. Eng.*, 2017, **61**, (2), pp. 102–108

doi: 10.1049/mnl.2018.5106